Directional Order Tracking in Rotating Machines

Izhak Bucher
Dynamics Laboratory,
Mechanical Engineering,
Technion—Israel Institute of Technology,
Haifa 32000, Israel
e-mail: bucher@technion.ac.il

This paper describes a computationally simple method to isolate transient vibration from rotating components whose frequency is tightly linked to rotation and to modes of vibration. The results can be viewed as an enhancement of computed order tracking or amplitude demodulation of multiple crossing frequency terms. By measuring the response with an array of sensors, one can compute the relative, instantaneous phase between different sensors and thus obtain information about the spatial behavior of different components with different wavelengths, frequencies, and traveling directions. An array of sensors would thus exploit spatial information to separate different vibration modes and thus gain deeper insight into the dynamical behavior. The proposed method is suitable for whirling shafts and rotating disk-like structures. It is computationally simple and fast while providing better separation of components than single sensor based approaches, in particular when ordinary methods fail to separate close frequencies. It is demonstrated that through the exploitation of cyclic symmetry of rotating structures and the angular periodicity of the vibration modes, the spectral contents of different modes can be separated. Simulated and measured data demonstrate the merits of the proposed algorithm.
[DOI: 10.1115/1.4024052]

Keywords: rotating structures, disk vibration, order tracking, shaft whirl, traveling waves, demodulation, signal envelope, signal processing, mistuning

1 Introduction

Rotating machines often exhibit transient vibrations whose frequency spectrum changes with speed of rotation. The most dominant components are often synchronous to the speed of rotation and its integral multiplications. These components are called engine-orders, and the task of isolating individual components is called order-tracking or now, with the advent of digital computations, "computed order-tracking." The extraction of engine-orders helps to isolate the source for excessive vibrations thus providing a focused diagnostic instrument. Integer or fractional multiples of rotation speed appear in faulty bearings, gears, an unbalanced shaft, or under parametric vibrations of rotating devices [1]. Mistuning, i.e., small differences between the jet-engine blades properties, can bring about large localized vibrations characterized by unique temporal and spatial behavior [2,3]. The current paper enhances order tracking in the case of whirling shafts and rotating disk-like structures by processing data coming from several sensors simultaneously thus putting more emphasis on the true physical behavior of the system rather than relying only on the apparent frequencies. By distributing a number of sensors on the vibrating structure circumferentially, richer information than what a single sensor provides is gained. The spatial deployment provides information about the relative phase between the measured locations thus enabling the separation of otherwise overlapping variable-frequency components. The separation procedure can isolate components according to the direction the vibration waves propagate [4–6] and according to their spatial wavelength in addition to separating different frequencies. The proposed method is computationally simple and robust.

Rotating machine vibrations are often the local manifestation of circumferentially traveling stress waves excited by the interaction between stationary and rotating parts. Different waves may have close apparent frequencies, despite being excited by different physical modes. Different components may have crossing frequency terms [5] that cause artificial modulations in standard order-tracking procedures [7] due to the limited resolution and the inherent ambiguity. The proposed approach can separate close and crossing frequency terms accurately, as long as they belong to different types of traveling waves [8]. Furthermore, the proposed method exploits the phase information to project measured vibrations onto rotating and body-fixed coordinates in transient conditions thus shedding more light on the true nature of the elastic deformations and stress levels and on mistuning [2,3]. Having separated the engine orders, these can be subtracted from the measured response to expose features hidden underneath these components thus enhancing the resolution of the analysis.

Computed order tracking methods have recently regained popularity with the advent of inexpensive digital signal processors and suitable numerical procedures [9–11]. Tracking signal components having frequencies that are linearly dependent upon the speed of rotation provides a simplified insight into otherwise complex response signals. Vibrations in rotating machines stem chiefly from rotation itself [6,12–17]; therefore, tracking speed-dependent signal components may shed light on the source of vibration. Furthermore, order tracking enables technical staff to monitor the health of a machine [1,18] with little knowledge in signal processing and rotor dynamics.

Computed order tracking, in its basic form, is now an essential part of many vibration analysis packages and measurement systems. Forward and backward whirling of shafts has been treated extensively in the past [4,7], and the information provided by this separation is now clearly understood. Still the whirl sense information is seldom used in practice, and it is suggested that directional order tracking can simplify the interpretation of shaft whirl sense and its implications.

The evolution of amplitude with speed and frequency has been treated in the past with a signal processing tool called Zmod [19] or by computing the time-frequency distribution [20] of measured signals. The term Zmod has historical roots in the aero-engine industry because it used the z-axis rear connector on old oscilloscopes. This ancient technique has been replaced nowadays by methods providing similar information via digital signal processing approaches. Digital signal processing software, mostly employing the discrete Fourier transform (DFT), can produce waterfall display having the ability to separate forward and backward whirling shaft motions [7]. Expanding these ideas for the separation of multiple wavelengths, commonly found in disks,

Contributed by the Design Engineering Division of ASME for publication in the Journal of Vibration and Acoustics. Manuscript received September 3, 2012; final manuscript received March 11, 2013; published online June 19, 2013. Assoc. Editor: Philippe Velex.

results in the Zmod-like time-frequency information (see Ref. [19]) with the ability to separate different modes according to the number of modal diameters (i.e., wavelength) [16] and where negative frequencies symbolize waves traveling in an opposite direction to the disk rotation speed [6,21]. Unfortunately, the methods described in Refs. [5,19] provide averaged, frequency domain data, and vibration levels during rapid transients can thus be underestimated. Clearly, all the available methods to compute time-frequency distributions, whether based on the discrete Fourier transform, Wigner–Ville distribution, or wavelet decomposition (e.g., Ref. [19]), suffer from limited resolution.

A recent paper [22] proposed an approach circumventing the averaging processes associated with frequency domain methods [7] by performing the wave decomposition in the time domain. This is achieved at the cost of a somewhat complicated, dual-step procedure that isolates the time domain components associated with the individual waves traveling on the structure circumferentially.

Order tracking, under suitable conditions, can provide accurate estimates of the individual amplitudes without producing an overwhelming amount of information [9,10].

Most set-ups contain two sensors per shaft section, but without a suitable procedure this seemingly redundant setup is seldom exploited in order tracking. While two sensors are sufficient for shaft dynamics [5,16], more sensors are needed to analyze rotating disk analysis [19,22–24]. The importance of separating forward and backward shaft whirl motions has been well established in the past (e.g. Refs. [4,6]) while disk vibrating and rotating disk dynamics require a more elaborate approach (e.g. Refs. [25–27]) or larger number of sensors to decompose the vibrations, as has been shown before [19,22]. The present problem is similar to what was presented in Ref. [28] but with an extension to multiple wavelength as in Ref. [22].

This paper proposes a compromise between simple spectrograms or waterfall diagrams [5,16,19], standard order tracking [5, 9–11,29], and elaborate computationally intensive time-domain methods [22].

Section 1 presents the motivation and provides some background material. The mathematical background and derivation of the proposed method from analytical and numerical perspectives are outlined in Sec. 2. The same part describes a numerical implementation of the method, and finally Sec. 3 demonstrates the proposed method on simulated and experimentally obtained data. The paper concludes with a brief discussion and summary.

2 Directional Order Tracking Algorithm and Implementation

Consider a rotating part undergoing dynamic deformations, such as illustrated in Fig. 1. The proposed separation method relies on the ability to simultaneously analyze data measured from several sensors. Normally the signal measured by a single sensor is analyzed, and the need for a method decomposing the individual parts of the signal is exemplified by a sample signal shown in Fig. 2.

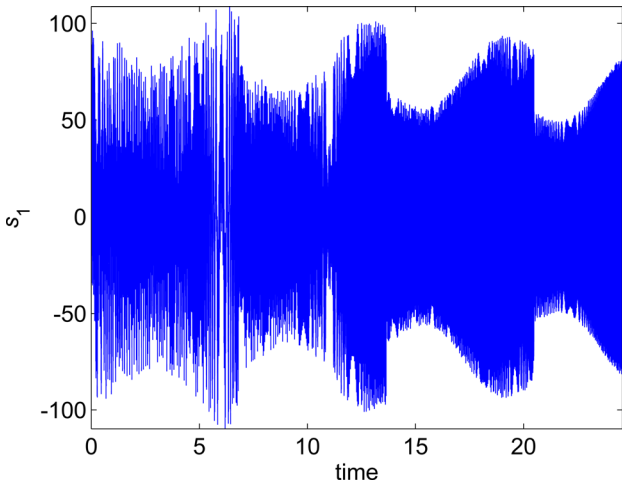

Fig. 2 Time response of $s_1(t)$ containing several components according to Eq. (20)

The effect of rotation as measured on the system depicted in Fig. 3 is clearly visible in Fig. 4 where the measured frequencies change with speed. Still, there are overlapping lines caused by different mechanisms and a slight indication of flutter beginning at 50 s (indicated by an erratic change of frequency with time). The color-coded figure shows that several components, probably resulting from different modes of vibration and different sources, overlap with no real ability to isolate them.

Clearly, the lack of spectral resolution [1,30] makes it rather difficult to find the cause for high vibrations in the low frequency region. With an array of sensors such as shown in Figs. 1 and 2, better separation can be achieved as shown below. The complicated plot in Fig. 4 is often replaced by tracking certain frequency lines, i.e., engine orders (EO). Indeed, in the case of disk-like vibrations, EO are not easily separated as they tend to cross several frequency lines (see Fig. 4) resulting from natural modes of vibration. The proposed approach attempts to combine the easy-to-decipher EO plots with two additional levels of separations, namely separation according to specific modes of vibration and according to the direction of rotation.

2.1 Spatial Decomposition of Orders—Demodulation. Vibrations measured on rotating structures during acceleration can be rather complex in the time and in the frequency domains. In

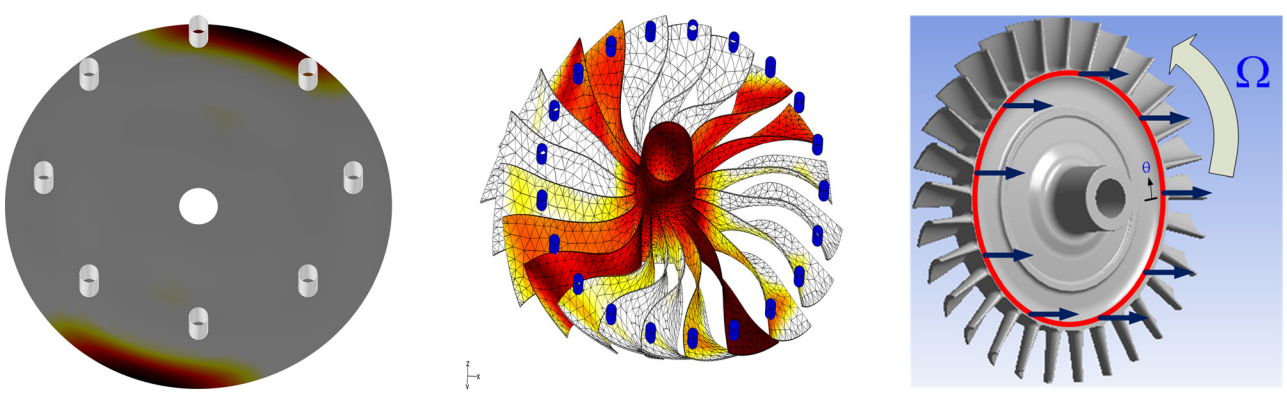

(a) (b) (c)

Fig. 1 Rotating disk with a circular array of sensors, engine fan model with illustrated array of sensors, and a bladed disk with continuous (circle) and discrete sensors (arrows)

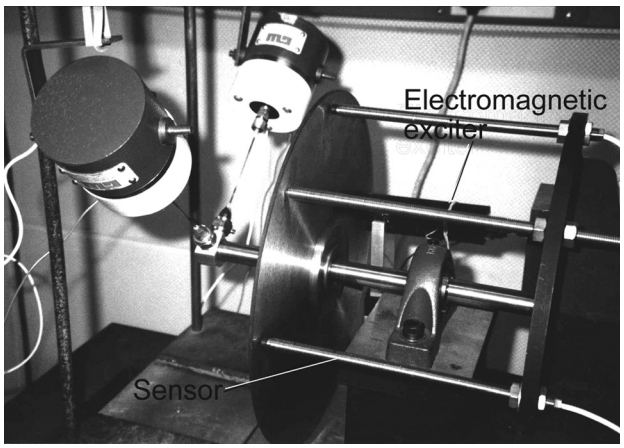

Fig. 3 A rotating disk with a stationary array of eight sensors

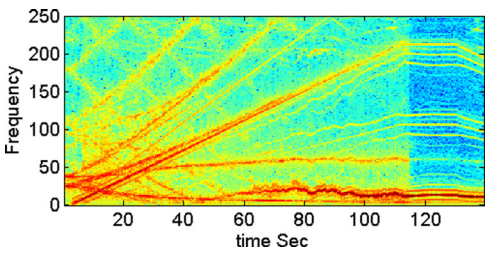

Fig. 4 A spectrogram computed with a single sensor during acceleration

the time domain, modes of vibration are excited simultaneously to gives rise to multifrequency, nonstationary response signals. In the frequency domain, amplitudes and frequencies are smeared due to the nonstationary nature of the phenomena. For this reason, methods capable of describing evolutionary spatial contents are often adopted [31,32]. Unfortunately, speed-frequency-amplitude maps or time-frequency distributions [5,20] can contain densely populated, often overlapping components and, therefore, the ability to understand the extent and the physical significance of individual components can be difficult. An effective approach to isolate single components according to their instantaneous frequency uses order tracking [9,10,33]

In this section, the analytical and mathematical background describing how any order tracking method can be enhanced to further separate close and crossing components effectively by exploiting the physical behavior of rotating structures is explained.

A sensor placed at a fixed angular location denoted by θ_j produces a signal described by

$$s_j(t) = \sum_{k=1}^{N} A_{kj}(t)\sin\varphi_k(t) + B_{kj}(t)\cos\varphi_k(t) + r_j(t) \quad (1)$$

The signal is modeled by (slowly or low-pass) time varying amplitudes $A_{kj}(t)$, $B_{kj}(t)$ and by the instantaneous phases $\varphi_k(t)$. The residual part $r_j(t)$ contains frequencies not included in this model and random nondeterministic components. Every modeled component has a time-varying frequency defined by [34]

$$\omega_k(t) = \frac{d\varphi_k(t)}{dt} \quad (2)$$

Here $\varphi_k(t)$ is the instantaneous phase of the signal, and $\omega_k(t)$ represents the instantaneous frequency of a specific narrow-band, isolated component of the dynamics.

In some cases, the frequency of the component is an integer multiple of rotation speed, i.e., $\omega_k(t) = n\Omega(t)$ where $n = 1, 2, 3,\ldots$. In these cases, $\varphi_k(t)$ represents the rotational phase and the integer multiples are referred to as engine orders. Transmissions and gears often give rise to a noninteger multiplier n. Rotating machines exhibit speed-dependent natural frequencies [6,14,15], and a certain mode of vibration can thus exhibit speed and, therefore, time dependent behavior. The instantaneous frequency, in these cases, is linked to a certain (or several) mode(s) of vibration and its dependence on the speed of rotation can be found by detailed analytical or numerical modeling [6,35], or simply by approximation and curve-fitting data generated by speed-frequency diagrams [5,7,36].

Order tracking isolates the amplitudes $A_{kj}(t)$, $B_{kj}(t)$ related to the signal component with phase $\varphi_k(t)$ and frequency $\dot{\varphi}_k(t)$. In disk-like structures, the amplitudes emanate from several modes of vibration, some of which have different numbers of modal diameters, these different modes are represented by the subscript j in Eq. (1) but all share the same instantaneous phase.

A simplified diagrammatic illustration of demodulation and frequency tracking is depicted in Fig. 5. The process of obtaining the slowly varying amplitudes of a faster sinusoidal term is called demodulation [37] and is now often realized by adaptive digital signal processing techniques [9–11,33].

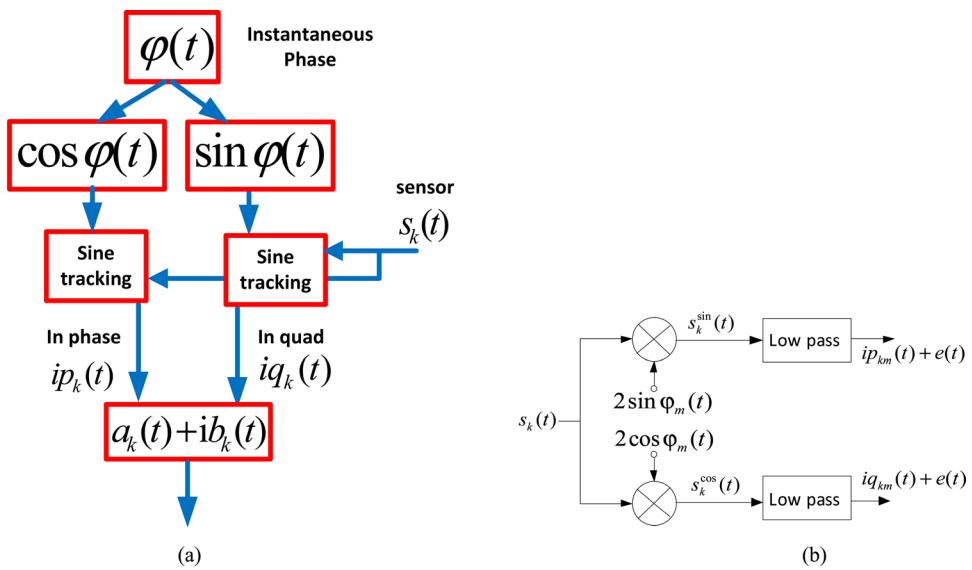

Fig. 5 Basic quadrature demodulation or order tracking of the *m*th engine order from the *n*th sensor—graphical representation

2.2 Measured Signals and Rotationally Traveling Waves of Cyclic Structures. An informative description of a signal measured from a rotating structure takes into consideration the dynamics of cyclically symmetric structures [38,39]. Owing to the cyclic symmetry of most rotating objects, circumferentially traveling waves arise naturally. Consider a typical rotating element, as shown in Fig. 1, undergoing elastic vibrations.

A typical bladed disk is shown in Fig. 1 where a hypothetical circumferentially continuous sensor measuring the response indicated by $s(\theta, t)$ is placed at a fixed radius in Figs. 1 and 2. A more realistic array of equispaced point-sensors is illustrated by the discrete sensors (arrows) drawn at the same radius. In order to analyze the circumferential separation, a continuous sensor that would measure a signal composed of the contribution of many modes, is assumed. Some modes of vibration are separated here according to their number of nodal diameters (ND) [40,41]. Having assumed a continuously distributed sensor, the measurement at any angle can be expressed mathematical as

$$s(\theta,t)=\sum_{n=0}^{\infty} a_n(t)\cos n\theta + b_n(t)\sin n\theta, \quad \theta\in[0,2\pi] \tag{3}$$

Rotating elements contain little damping, and therefore, the time varying amplitudes are composed of several amplitude-modulated narrow-band processes. These processes participate in the individual amplitudes of the nth nodal diameter modes, according to

$$\begin{aligned} a_n(t) &= \sum_{k=1}^{N} \tilde{A}^c_{kn}(t)\cos\varphi_{kn}(t) + \tilde{A}^s_{kn}(t)\sin\varphi_{kn}(t) \\ b_n(t) &= \sum_{k=1}^{N} \tilde{B}^c_{kn}(t)\cos\varphi_{kn}(t) + \tilde{B}^s_{kn}(t)\sin\varphi_{kn}(t) \end{aligned} \tag{4}$$

The functions $\tilde{A}^c_{kn}(t), \tilde{A}^s_{kn}(t)$, $\tilde{B}^c_{kn}(t)$, and $\tilde{B}^s_{kn}(t)$ are low-pass and $\dot{\varphi}_{kn}(t)$ is the instantaneous frequency of the kth component, which is associated with the n-ND modes. Substituting Eq. (4) in Eq. (3), one obtains

$$\begin{aligned} s(\theta,t) = \sum_{n=0}^{\infty} &\left(\sum_{k=1}^{N} \tilde{A}^c_{kn}(t)\cos\varphi_{kn}(t) + \tilde{A}^s_{kn}(t)\sin\varphi_{kn}(t)\right)\cos n\theta + \cdots \\ &+ \left(\sum_{k=1}^{N} \tilde{B}^c_{kn}(t)\cos\varphi_{kn}(t) + \tilde{B}^s_{kn}(t)\sin\varphi_{kn}(t)\right)\sin n\theta \end{aligned} \tag{5}$$

Employing trigonometric identities, Eq. (5) can be transformed into a traveling-waves representation

$$\begin{aligned} s(\theta,t) = \sum_{n=0}^{\infty}\sum_{k=1}^{N} &\left(\tilde{A}^c_{kn}(t) + \tilde{B}^s_{kn}(t)\right)\cos(\varphi_{kn}(t) - n\theta) \\ &+ \left(\tilde{B}^c_{kn}(t) - \tilde{A}^s_{kn}(t)\right)\sin(\varphi_{kn}(t) - n\theta) + \cdots \\ &+ \left(\tilde{A}^c_{kn}(t) - \tilde{B}^s_{kn}(t)\right)\cos(\varphi_{kn}(t) + n\theta) \\ &+ \left(\tilde{B}^c_{kn}(t) + \tilde{A}^s_{kn}(t)\right)\sin(\varphi_{kn}(t) + n\theta) \end{aligned} \tag{6}$$

A concise representation of Eq. (6) uses complex or phasor notation

$$s(\theta,t) = \Re\sum_{n=0}^{\infty}\sum_{k=1}^{N} A^+_{kn}(t)e^{\mathrm{i}(\varphi_{kn}(t)-n\theta)} + A^-_{kn}(t)e^{\mathrm{i}(\varphi_{kn}(t)+n\theta)} \tag{7}$$

Now, separating the amplitudes of the forward and backward traveling waves [19], one can write

$$\begin{aligned} A^+_{kn}(t) &\triangleq \frac{1}{2}\left(\left(\tilde{B}^s_{kn}(t) + \tilde{A}^c_{kn}(t)\right) + \mathrm{i}\left(\tilde{B}^c_{kn}(t) - \tilde{A}^s_{kn}(t)\right)\right), \\ A^-_{kn}(t) &\triangleq \frac{1}{2}\left(\left(\tilde{A}^c_{kn}(t) - \tilde{B}^s_{kn}(t)\right) - \mathrm{i}\left(\tilde{A}^s_{kn}(t) + \tilde{B}^c_{kn}(t)\right)\right) \end{aligned} \tag{8}$$

The functions $A^+_{kn}(t), A^-_{kn}(t)$ are the slowly varying (complex) amplitudes (i.e., low-pass [34]) of the corotating (forward) and counter rotating (backward) waves, respectively. The instantaneous frequencies $\dot{\varphi}_{kn}(t)$ describe general time-dependent (smoothly varying) functions that could trace any smooth curve in the time-frequency domain; see Ref. [42] for discussion on time-varying frequencies.

2.3 Tracking Engine Orders With Continuous and Discretely Placed Sensors. An array of N sensors is deployed around the rotating and vibrating disk-like structure, as shown in Figs. 1 and 2. Consider isolating the components related to phase $\varphi_{k_0 n}(t)$ by means of co/quad demodulation. Rewriting Eq. (5) in co/quad form, one obtains

$$\begin{aligned} s(\theta,t) = \sum_{n=0}^{\infty} &\left(\tilde{A}^c_{k_0 n}(t)\cos n\theta + \tilde{B}^c_{k_0 n}(t)\sin n\theta\right)\cos\varphi_{k_0 n}(t) + \cdots \\ &+ \left(\tilde{A}^s_{k_0 n}(t)\cos n\theta + \tilde{B}^s_{k_0 n}(t)\sin n\theta\right)\sin\varphi_{k_0 n}(t) \end{aligned} \tag{9}$$

By employing standard demodulation to obtain the in-phase part of the sensor, one has

$$ip_{k_0}(\theta,t) = \sum_{n=0}^{\infty}\left(\tilde{A}^c_{k_0 n}(t)\cos n\theta + \tilde{B}^c_{k_0 n}(t)\sin n\theta\right) \tag{10}$$

and the in-quadrature is

$$iq_{k_0}(\theta,t) = \sum_{n=0}^{\infty}\left(\tilde{A}^s_{k_0 n}(t)\cos n\theta + \tilde{B}^s_{k_0 n}(t)\sin n\theta\right) \tag{11}$$

Equations (10) and (11) combine the amplitudes of all the disk modes and are the result of standard order tracking procedures, whose basic form is illustrated in Fig. 4. Making use of the cyclic nature of the structure, one can apply a spatial Fourier transform to obtain

$$\tilde{A}^c_{k_0 n}(t) = \frac{1}{\pi}\int_0^{2\pi} ip_{k_0}(\theta,t)\cos n\theta d\theta, \quad \tilde{B}^c_{k_0 n}(t) = \frac{1}{\pi}\int_0^{2\pi} ip_{k_0}(\theta,t)\sin n\theta d\theta \tag{12}$$

$$\tilde{A}^s_{k_0 n}(t) = \frac{1}{\pi}\int_0^{2\pi} iq_{k_0}(\theta,t)\cos n\theta d\theta, \quad \tilde{B}^s_{k_0 n}(t) = \frac{1}{\pi}\int_0^{2\pi} iq_{k_0}(\theta,t)\sin n\theta d\theta \tag{13}$$

Resorting to an equispaced array of sensors with $\theta = \frac{2\pi p}{N}$, $p = 0, 1 \ldots N-1$, one can obtain the individual components via DFT (assuming there is no spatial leakage, [1])

$$\begin{aligned} \tilde{A}^c_{k_0 n_0}(t) &= \frac{2}{N}\sum_{p=0}^{N-1}\left(ip_{k_0 p}(t)\cos n_0\frac{2\pi p}{N}\right), \\ \tilde{B}^c_{k_0 n_0}(t) &= \frac{2}{N}\sum_{p=0}^{N-1}\left(ip_{k_0 p}(t)\sin n_0\frac{2\pi p}{N}\right) \\ \tilde{A}^s_{k_0 n_0}(t) &= \frac{2}{N}\sum_{p=0}^{N-1}\left(iq_{k_0 p}(t)\cos n_0\frac{2\pi p}{N}\right), \\ \tilde{B}^s_{k_0 n_0}(t) &= \frac{2}{N}\sum_{p=0}^{N-1}\left(iq_{k_0 p}(t)\sin n_0\frac{2\pi p}{N}\right) \end{aligned} \tag{14}$$

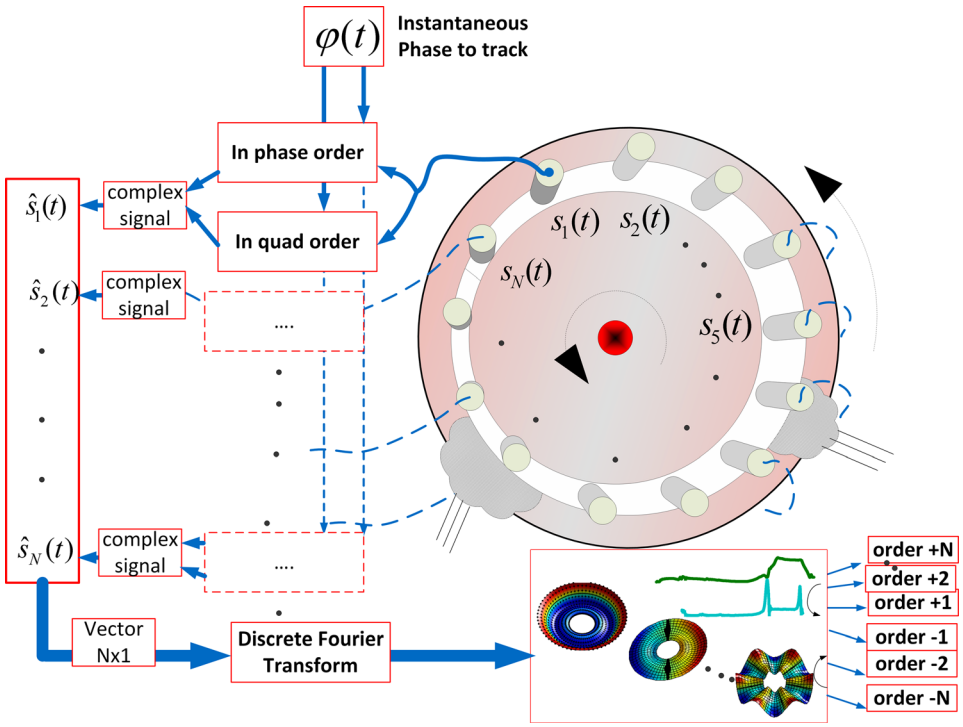

Fig. 6 Graphical representation of the multidimensional, directional order-tracking procedure

Finally, one can employ Eq. (8) to estimate the forward and backward parts of the EO associated with $\varphi_{k_0 n}(t)$. The entire procedure resulting from the proposed mathematical development is illustrated graphically in Fig. 6. Figure 6 is realized by implementing the scalar demodulation of Fig. 5 followed by wavelength separation with Eq. (14). The directional information is found by substituting the outcome of Eq. (14) in Eq. (8).

2.4 Moving Coordinate Systems, Apparent and Shifted Frequencies. It is often desired to relate the measurement taken by an array of sensors at one coordinate system (CS) to a system rotating with a relative phase angle of $\Psi(t)$. It is assumed that rotation is in the positive θ direction; thus, denoting ϕ as a fixed angle measured relative to the rotating CS, it is straightforward to relate these angles via [43]

$$\phi = \theta + \Psi(t) \tag{15}$$

When transforming between stationary and body-fixed coordinates, the relative angle is computed with the instantaneous rotation speed $\Omega(t)$ according to

$$\Psi(t) = \int_0^t \Omega(\tau) d\tau \tag{16}$$

Substituting Eq. (15) in Eq. (7), one can obtain an expression for the signal a fictitious sensor residing at (r_0, ϕ) in the rotating CS would measure

$$\begin{aligned} {}_b s(\phi, t) &= s(\theta + \Psi(t), t) \\ &= \Re \sum_{n=0}^{\infty} \sum_{k=1}^{N} A_{kn}^{+}(t) e^{\mathrm{i}(\varphi_{kn} - n\Psi)} e^{-\mathrm{i}n\phi} + A_{kn}^{-}(t) e^{\mathrm{i}(\varphi_{kn} + n\Psi)} e^{\mathrm{i}n\phi} \end{aligned} \tag{17}$$

The apparent frequencies, as evident from Eq. (17), change for every EO (or phase component), when transformed to the body-fixed CS. Indeed it depends on the direction and on the ND of the individual component, via

$$\omega_n^{+} = \dot{\varphi}_{kn}(t) - n\Omega(t), \quad \omega_n^{-} = \dot{\varphi}_{kn}(t) + n\Omega(t) \tag{18}$$

One can relate the engine orders measured in stationary coordinates to the frequencies a sensor would measure in body-fixed coordinates, by using the fact that EO of different ND travel at different angular speeds (cf. Eq. (18)). The specific number of ND does not change for the individual components; thus one can make use of Eqs. (17) and (18) to estimate what a material point is actually experiencing in body-fixed coordinates.

Having isolated $A_{kn}^{+}(t), A_{kn}^{-}(t)$ as shown above, it is possible to transform individual components to body-fixed CS with

$$A_{kn}^{+}(t) e^{\mathrm{i}(\varphi_{kn} - n\Psi)}, \quad A_{kn}^{-}(t) e^{\mathrm{i}(\varphi_{kn} + n\Psi)} \tag{19}$$

Although the EO computed by Eq. (14) are low-pass (slow), in the body CS, the apparent frequencies of these components do change as will be demonstrated later on.

The entire procedure is based on the scalar demodulation stage as represented by the transition from Eq. (9) to Eqs. (10) and (11) according to any scalar order-tracking approach (e.g., Fig. 5). This process, unlike the subsequent stages, involves some approximation and is based on some assumptions about the signal bandwidth, and it involves nonlinear or nonstationary filtering.

3 Numerical and Experimental Examples

This section presents simulated and experimentally based case-studies of the proposed method. The first example includes synthetic time-varying signals with forward and backward traveling waves having different wavelengths. These components intersect in the time-frequency domain and, therefore, ordinary order-tracking could fail, whereas the proposed method shows better separation of the individual components. Experimental results begin with shaft vibration decomposition, and later rotating disk vibrations are analyzed in stationary and rotating coordinates. Finally, a simulated cyclically-symmetric structure with different

levels of mistuning is numerically simulated to discuss the use of the proposed approach in quantifying imperfections.

3.1 Simulated Example. Consider a rotating and vibrating disk whose dynamics are measured by $N=7$ equispaced sensors as shown in Figs. 1 and 2. The simulated measurements for each one of the sensors are computed via

$$s(\theta,t)=\sum_{r=1}^{4}A_r(t)\cos(\varphi_r(t)-n_r\theta),$$
$$s_k(t)\overset{\Delta}{=}s(\theta,t)|_{\theta=(2\pi k)/7},\quad k=0\ldots6 \tag{20}$$

The instantaneous phase of each of the four components, representing either run-up or run-down of the rotating system, obeys

$$\varphi_r(t)=\omega_r t+\gamma_1 t^2+\gamma_2 t^3, r=1\ldots4 \tag{21}$$

and the parameters determining the instantaneous amplitude and phase are given in Table 1.

The simulated response at one of the sensors is shown in Fig. 2. Clearly, the signal, being composed of several nonsynchronous and nonstationary components, looks rather erratic. One can notice from the time-frequency map of this signal (see Fig. 7) and from Table 1 that several modes participate in the same component and several orders intersect in Fig. 7. The example attempts to isolate all the components related to a single phase term $\varphi_2(t)$. Initially order tracking is applied to a single sensor and later to all sensors simultaneously. The results are shown in Fig. 8, and several conclusions can be made. With a single sensor (indicated by s_1), misleading results were obtained. The multisensor clearly isolates the instantaneous amplitudes associated with $n=-3,+2$ nodal diameters quite well. As for the other terms, small spikes in amplitudes arise whenever term crossing occurs, but these spikes, unlike the true terms, are very sensitive to the nonlinear demodulation procedure and can thus be identified by altering the bandwidth of the demodulation process (as defined in Refs. [9,11]). Having identified the true components, one can subtract them from the original signals and proceed with the component identification by "peeling" component by component. An example for this procedure will be shown for real data later on.

3.2 Experiments—Rotating Shaft and Disk. Shaft disk vibrations were measured on a laboratory test-rig (see Figs. 2 and 9), and the directional decomposition is demonstrated in several ways:

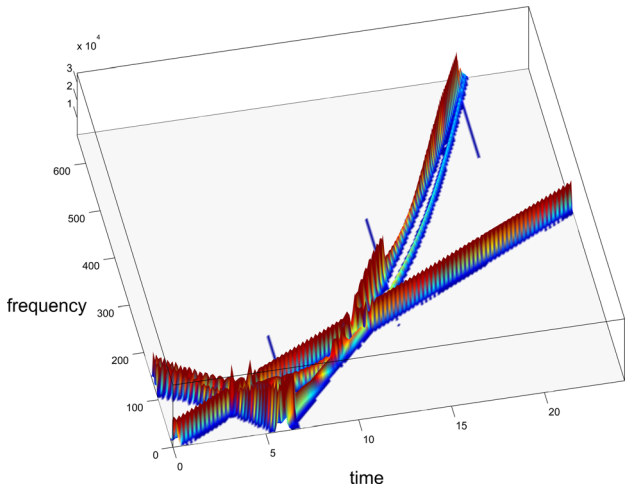

Fig. 7 Waterfall (spectrogram) representation of the signal in Fig. 2 and Eq. (20)

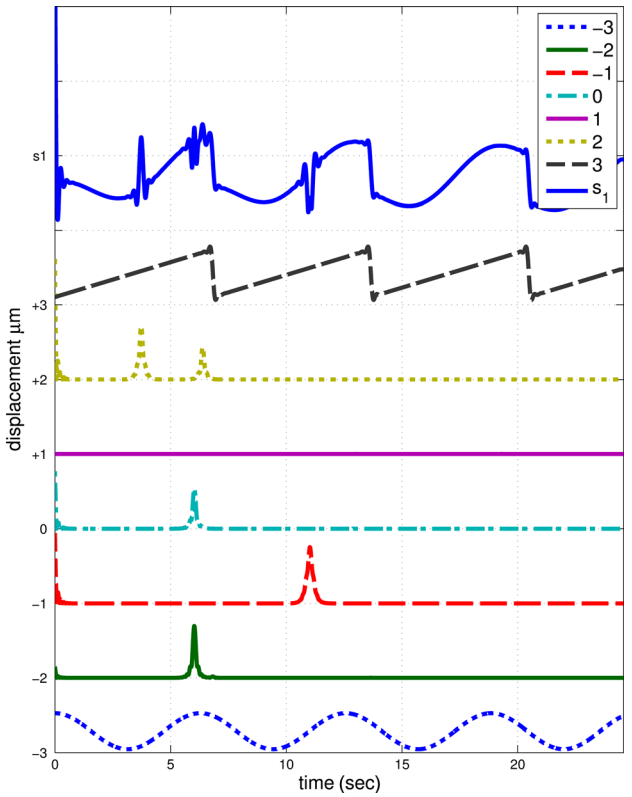

Fig. 8 Extracted spatial vibration components along $\varphi_2(t)$ from a simulated rotating disk using seven sensors. Also shown is the attempt to track this order with a single sensor, $s_1(t)$ (shifted for clarity—continuous line) and the spatially decomposed components with nodal diameters in the range (–3 ··· +3).

(i) a simple forward and backward decomposition of the shaft whirl in the time domain making use of two sensors measuring the shaft bending
(ii) decomposition of the various disk modes with an array of $N=8$ sensors spread at equispaced angles along a flexible disk and transformed to the body-fixed coordinates a material point on the disk senses
(iii) subtracting all rotationally driven engine orders with an array of $N=4$ to reveal the underlying dynamics

The experimental system, shown in Fig. 9 consisted of a 20 mm diameter flexible shaft, which was 1.0 m long. The shaft was mounted on two self-aligning ball-bearings, and it was driven by a 20 Nm rated AC brushless motor capable of running up to 4500 RPM. A flexible disk was mounted on the other end of the shaft. In the present test, an active magnetic bearing produced a small, band limited random force to enrich the measurements and simulate the effect of turbulence in real jet-engines. Not shown in Fig. 9 is the sensor array measuring the disk vibration in a similar arrangement to Fig. 2.

3.2.1 Separating the Direction of Wave Travel—A Whirling Shaft. Normally, for a rotating shaft, two sensors are placed at 90 deg. Indeed, the system in Fig. 9 has two sensors $s_0(t)$, $s_1(t)$ at 0 deg and 90 deg, respectively. In order to apply Eq. (14), one can make use of the fact that

$$s_2(t)=-s_0(t),\quad s_3(t)=-s_1(t) \tag{22}$$

(see Fig. 7 and Appendices C and D in Ref. [36]) thus producing an effective array containing $N=4$ sensors displaced 90 deg apart.

The shaft was accelerated beyond the first critical speed, and the instantaneous phase of rotation was recorded in addition to $s_0(t)$, $s_1(t)$.

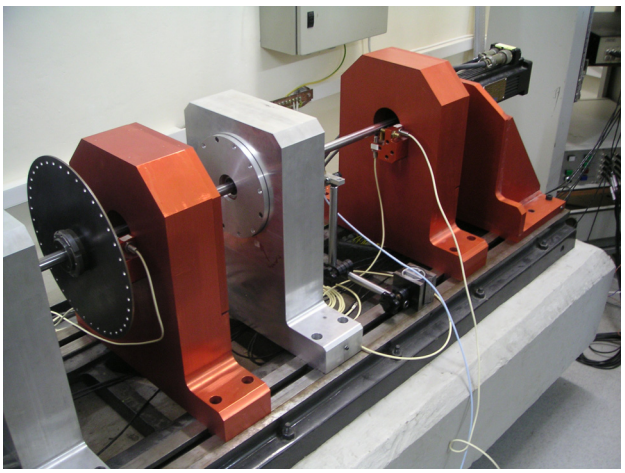

Fig. 9 Laboratory system showing rotating disk, two shaft sensors

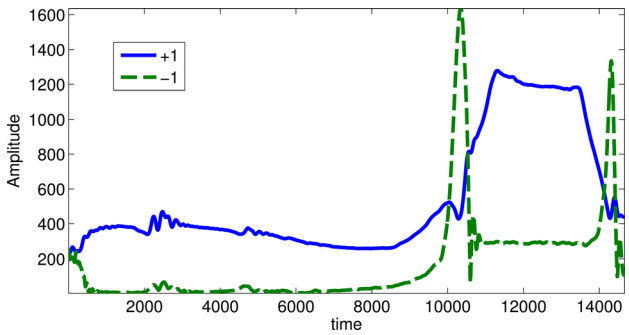

Fig. 10 Forward and backward components of order 1, $\dot{\varphi}(t) = \Omega(t)$ for the vibrating shaft during speed change. Measured on the system in Fig. 9.

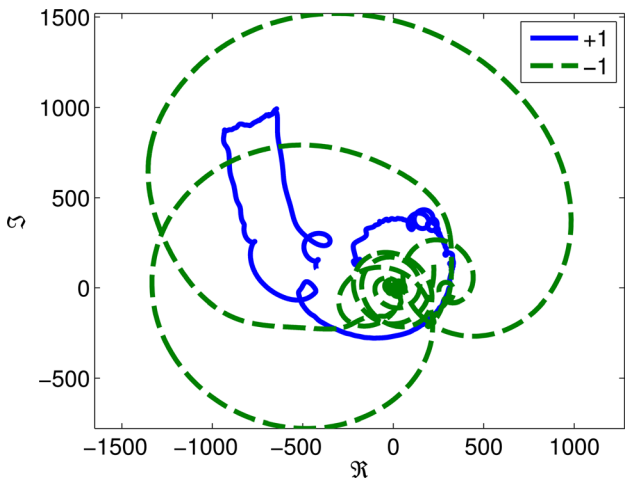

Fig. 11 Complex amplitudes (see Fig. 10) of the forward and backward whirl along the first engine-order (EO-1, $\dot{\varphi}(t) = \Omega(t)$) measured with two sensors on the system in Fig. 9 during rotation speed change

Substitution of Eq. (22) in Eq. (14) shows that $A_{0n}(t) = A^{\pm}_{2n}(t) \equiv 0$ (see also Ref. [19]). We are thus left with the components with $k = 1$ nodal diameters, i.e., $A^{\pm}_{1n}(t)$. The amplitude and complex versions of the instantaneous amplitudes are computed with Eq. (14) for the first EO, i.e., $\varphi_1(t) = \Omega t$, with Ω being the instantaneous rotation speed.

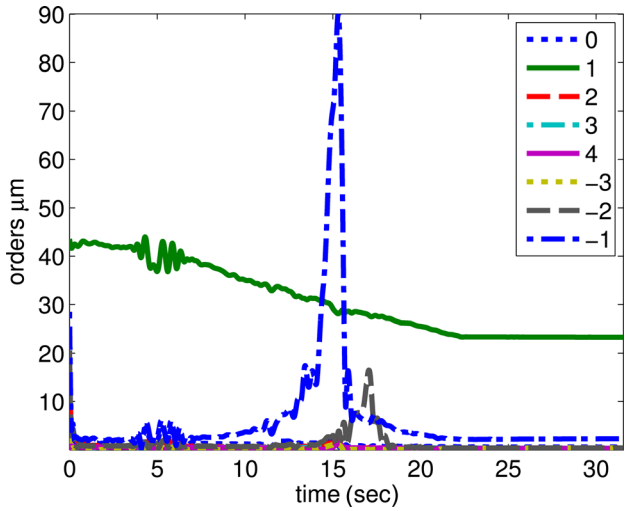

Fig. 12 Engine orders of a rotating disk for EO-1 in inertial coordinates using eight equally-spaced sensors as in Fig. 2 but measured on the system in Fig. 9

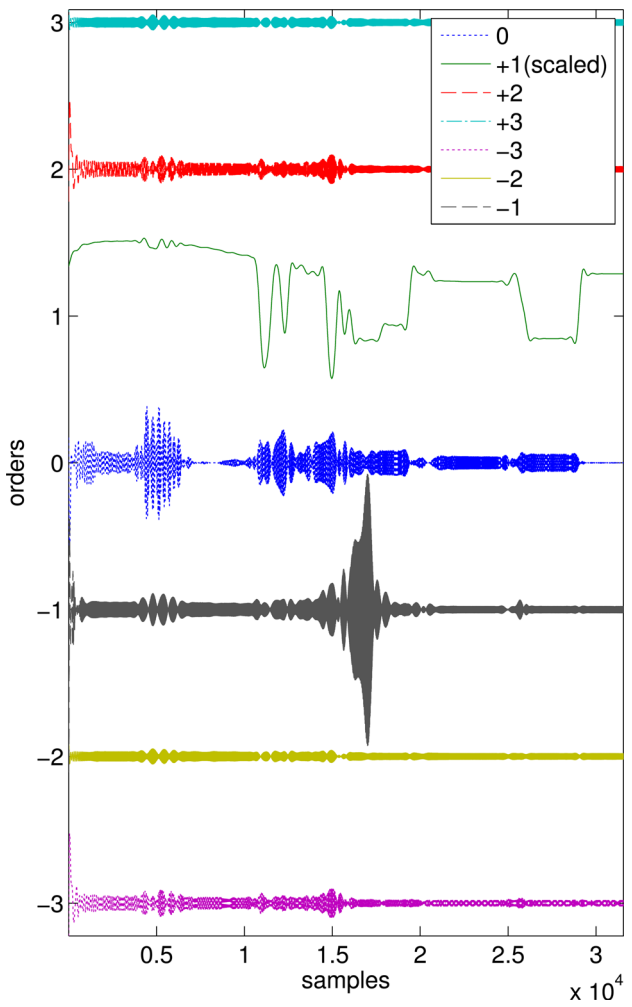

Fig. 13 Decomposed spatial components of EO-1 vibrations measured on a rotating disk transformed to body-fixed coordinates

It is surprising to note in Fig. 10 that the backward whirl motion (−1) has larger amplitude than the forward term (+1) despite being excited by a forward rotating unbalance. This fact is important because the forward term presents nearly static deformation

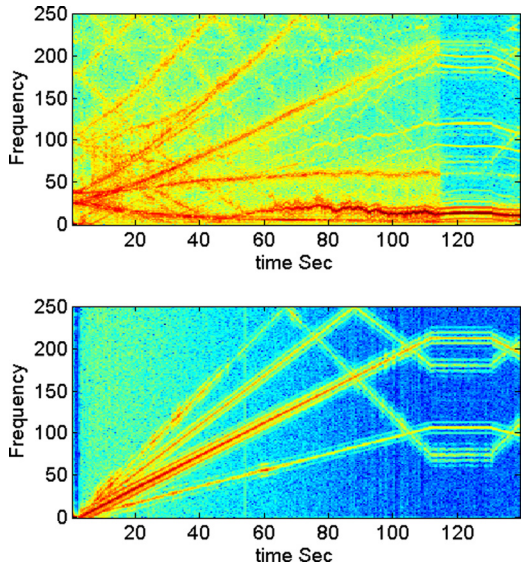

Fig. 14 Subtracting engine orders: original Fig. 4, bottom: subtracted orders (combined), top: resulting spectrogram after subtracting EO-1…4, inertial coordinates

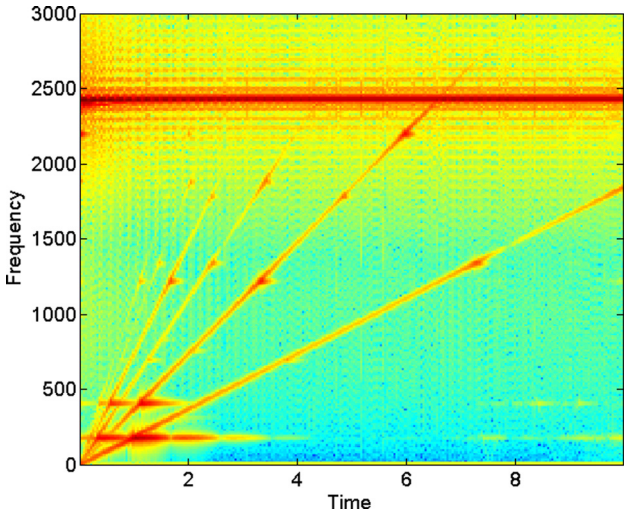

Fig. 16 Time-frequency map measured on a single blade in a direction normal to the blade while the force in Eq. (24) was acting on the system from Fig. 15. Note the abrupt increase in amplitude (indicated by local color changes) upon excitation of modes by the engine-orders.

in body-fixed coordinates while the backward term oscillates twice per revolution (e.g., see Ref. [14]). Coquad or complex demodulation produces complex amplitudes and indeed, Fig. 11 traces the real versus imaginary amplitudes (or orders) showing that phase changes rapidly for the forward term (+1), while being rather stationary around the critical speed for the (–1) term.

3.2.2 Decomposition in Inertial Coordinates. The proposed decomposition was applied to an array of $N = 8$ stationary sensors for tracking, $\varphi_1(t) = \Omega t$. The results shown in Fig. 12 trace the amplitudes for different wavelengths versus time measured. The result shows that in inertial coordinates, the (+1,–1,–2) terms have meaningful amplitudes where the (+1) shows no special increase near the critical speed, while (–1) shows a large resonant amplitude when crossing the backward natural frequency. Clearly, without the decomposition, it is impossible to separate the static (+1) component from the oscillating (–1) part.

3.2.3 Transforming the Decomposition Into Body-Fixed Coordinates. One can produce simulated time signals for fictitious sensors glued to the disk with Eq. (19). Indeed, the original time functions as obtained in inertial coordinates are now transformed to yield Fig. 13. In body fixed coordinates the (+1) component along $\varphi_1(t) = \Omega t$ is nearly constant. This term is mostly affected by the disk's initial wobbliness, which flattens with speed (see Fig. 12). The backward going components (–1,–2) seem more meaningful, and the true alteration of strain and stress can be computed with this newly computed data. It should be emphasized that the decomposition is essential for the proposed transformation since different wavelengths travel at different speeds.

3.2.4 Subtracting Selected Orders From Measured Data. Certain time varying components can obscure other terms that are hidden or masked in the time-frequency domain. In this example, $N = 4$ sensors were used to remove four engine orders, i.e., $\varphi_n(t) = n\Omega t, n = 1\ldots4$. Being able to separate the forward and backward traveling components, one can subtract these terms from the original signals by creating "holes," i.e., without affecting terms having different numbers of nodal diameters or crossing frequency terms. The time-frequency distribution of the original signals is depicted in Fig. 4 where the influence of the EOs is clearly visible. The first stage involved the identification of the engine orders according to the proposed procedure and creating suitable time functions describing the forward and backward terms for all the nodal diameters. These terms are subsequently removed from the original signals, and the results are shown in Fig. 14. Clearly, the EO terms that are shown at the bottom were removed to create Fig. 14—top and better visibility of the natural frequency has been achieved with no holes in their description due to the clean removal of the engine orders 1–4.

3.3 Simulation of a Mistuned Cyclically Symmetric Structure. Rotating structures are often cyclically-symmetric and any small deviation in the properties of individual sectors (i.e., blades as shown in Figs. 1 and 15) can give rise to elevated vibration levels in some configurations. It is well known that the transition from pure axisymmetry to cyclic symmetry "contaminates" modes having N nodal diameters with other modes having (say) k ND. With perfectly identical sectors, modes of vibration can have $N \pm k$ ND (e.g., see Ref. [39]). These

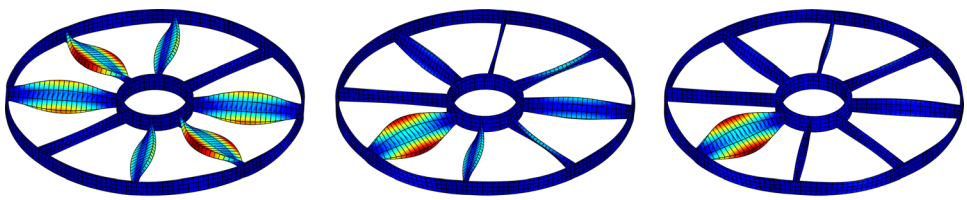

Fig. 15 A Finite element model of a mistuned structure with cyclic-symmetry. Showing one mode under different levels of mistuning (from left to right): (i) near perfect, no mistuning, (ii) 3% blade thickness variations, and (iii) 9% blade thickness variations.

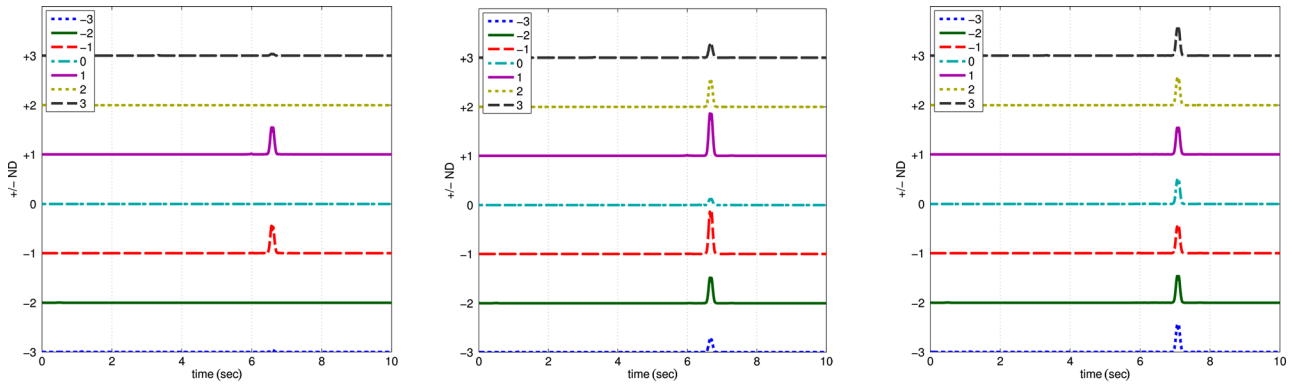

Fig. 17 A single engine order at $2\times\Omega$ (2EO) decomposed into contribution of several nodal diameters in the range ND = −3...3. The plots correspond to the systems depicted in Fig. 15 where (i) left: near perfect, no mistuning, (ii) middle: 3% mistuning of random blade thickness variations, and (iii) right: 9% blade or random thickness variations.

structures can start their lives with near perfect cyclic-symmetry and degenerate, due to wear, into mistuned structures exhibiting a different dynamical behavior. In this case, the distinct spatial pattern is distorted and additional wavelengths (ND) appear. The present simulation demonstrates that spatial decomposition can be used to detect this feature by isolating the appearance of additional ND data in the measured response.

In order to excite all the modes, a rotating force was simulated such that it acts on the outer rim of the structure in the radial direction. The force changes in time to simulate speed run-up according to

$$f_r(\theta,t)=\exp\left(-10\sin^2\left(\frac{\theta-a_\Omega t^2}{2}\right)\right) \tag{23}$$

A single acceleration parameter, $a_\Omega=580$ determines the EO lines (see Fig. 16).

The specific selection of force distribution, which is localized in space, excites many nodal diameters simultaneously, as evident from Fig. 16. In order to illustrate the effect of mistuning on the proposed method, three finite element models were constructed. The effect of mistuning and the geometry of the structure can be viewed in Fig. 15 where different levels of mistuning were induced by changing the blades thickness. Observing the response of a signal blade during run-up does not reveal any difference between the three cases (tuned, 3% mistuning, 9% random mistuning). Clearly, the type of mistuning (mass, stiffness, thickness) and its spatial distribution affect specific modes more than others, depending on the projection of mistuning on the spatial displacement exhibited by the particular mode shape. Indeed, Fig. 5 shows that the perfectly cyclic structure exhibits $n=1$ nodal diameter circumferential variation. This fact was captured by the directional order tracking in Fig. 17. Upon crossing the natural frequency of the mode shown in Fig. 15, only +/–1 ND were excited having the same amplitudes thus indicating a standing wave in the structure. By introducing 3% thickness variation of the blades, a localized mode (middle plot in Fig. 15) was formed, but the +/–1 ND still prevail. Finally, the largest mistuning level shown on the right of Figs. 15 and 17 created a highly contaminated mode with equal amplitudes for all ND in Fig. 17. In the latter case, the mode exhibits the motion of a single blade (right plot in Fig. 15). Clearly, the decomposition of the response upon crossing a critical speed of any EO shows an indication for mistuning by detecting the increase of contaminating ND.

4 Discussion and Summary

The present paper discusses an enhanced order-tracking procedure that takes into account the spatial and directional features of vibration patterns. Given the deployment of a circumferentially equispaced array of sensors, the suggested approach produces richer decomposition than ordinary order tracking methods. The proposed method tracks a certain frequency or phase, which is changing with speed and time to extract the amplitude and phase information for several modes of vibration. With the proposed procedure, terms that have close frequencies, overlapping and crossing instantaneous frequencies can be effectively identified. Being able to reconstruct the time functions of the various components, one can selectively remove them from the original signals and assess their role, origin, and weigh their importance on the developing vibration. The proposed method is computationally simple and can be implemented in real-time. With the separation into different wavelengths or nodal diameters, stationary sensors can be used to assess vibration levels in material or body-fixed coordinates and thus provide a reliable measure of stress levels and detect mistuning in cyclically symmetric structures. Mistuning of cyclic structures can be identified by the appearance of contaminating nodal diameters in measured responses of mode-shapes as demonstrated via simulation.

Appendix

Table 1 Coefficients of the simulated disk measured data used in Eqs. (20) and (21)

r	n_r	ω_r	γ_r	γ_r	$A_r(t)$	comment
1	2	240π	−40	−2.5	$5.2+32\,f_{\text{saw}}\left(\frac{t}{1.738}\right)$	$f_{\text{saw}}(\alpha)\overset{\Delta}{=}\alpha-\left\lfloor\frac{\alpha}{2\pi}\right\rfloor$
2	−3	240π	−40	−2.5	14 12 cos(t)	same phase as $r=1$
3	−1	280π	−80	5	$35e^{-0.08t}$	close to $r=2$
4	1	0	15π	0	1.0	

References

[1] Braun, S., 1986, *Mechanical Signature Analysis: Theory and Applications*, Academic, New York.

[2] Judge, J., Pierre, C., and Mehmed, O., 2001, "Experimental Investigation of Mode Localization and Forced Response Amplitude Magnification for a Mistuned Bladed Disk," ASME J. Eng. Gas Turbines Power, **123**, pp. 940–950.

[3] Ewins, D., 1969, "The Effects of Detuning Upon the Forced Vibrations of Bladed Disks," J. Sound Vib., **9**(1), pp. 65–79.

[4] Lee, C. W., 1991, "A Complex Modal Testing Theory for Rotating Machinery," Mech. Syst. Signal Process., **5**(2), pp. 119–137.

[5] Han, Y. S., and Lee, C. W., 1999, "Directional Wigner Distribution for Order Analysis in Rotating/Reciprocating Machines," Mech. Syst. Signal Process., **13**(5), pp. 723–737.

[6] Genta, G., 2005, *Dynamics of Rotating Systems*, Springer, New York.

[7] Lee, C. W., and Han, Y. S., 1998, "The Directional Wigner Distribution and Its Applications," J. Sound Vib., **216**(4), pp. 585–600.

[8] Radcliffe, C., and Mote, C., Jr., 1983, "Identification and Control of Rotating Disk Vibration," ASME J. Dyn. Syst., Meas., Control, **105**(1), pp. 39–43.
[9] Fyfe, K., and Munck, E., 1997, "Analysis of Computed Order Tracking," Mech. Syst. Signal Process., **11**(2), pp. 187–205.
[10] Potter, R., 1990, "A New Order Tracking Method for Rotating Machinery," Sound Vib., **24**(9), pp. 30–34.
[11] Vold, H., and Leuridan, J., 1993, "High Resolution Order Tracking at Extreme Slew Rates, Using Kalman Tracking Filters," SAE Technical Paper 931288.
[12] Chen, W. J., and Gunter, E. J., 2005, *Introduction to Dynamics of Rotor-Bearing Systems*, Trafford, Bloomington, IN.
[13] Dimarogonas, A. D., and Paipetis, S. A., 1983, *Analytical Methods in Rotor Dynamics*, Elsevier, New York.
[14] Gasch, R., Nordmann, R., and Pfützner, H., 2002, *Rotordynamik*, Springer, New York.
[15] Lalanne, M., and Ferraris, G., 1998, *Rotordynamics: Prediction in Engineering*, Wiley, New York.
[16] Muszyńska, A., 2005, *Rotordynamics*, CRC, Boca Raton, FL.
[17] Vance, J. M., Murphy, B., and Zeidan, F., 2010, *Machinery Vibration and Rotordynamics*, Wiley, New York.
[18] Randall, R., 2011, *Vibration-Based Condition Monitoring: Industrial, Aerospace and Automotive Applications*, Wiley, New York.
[19] Bucher, I., Ewins, D., Robb, D., and Schmiechen, P., 1995, "Multi-Dimensional Directional Spectrograms and Campbell (ZMOD) Diagrams for Rotating Machinery," Proceedings of the 1995 ASME Design Engineering Technical Conference Part C, Boston, MA, October, Vol. 84, pp. 1327–1336.
[20] Cohen, L., 1995, *Time-Frequency Analysis: Theory and Applications*, Prentice-Hall, Englewood Cliffs, NJ.
[21] Schmiechen, P., 1998, "Travelling-Wave Speed Coincidence," Ph.D. thesis, Imperial College, London.
[22] Bucher, I., 2011, "Transforming and Separating Rotating Disk Vibrations Using a Sensor Array," J. Sound. Vib., **330**(6), pp. 1244–1264.
[23] Irretier, H., and Reuter, F., 1997, "Frequency Response Functions of Rotating Periodically Time-Varying Systems," Proceedings of the 15th International Modal Analysis Conference (IMAC XV), pp. 350–356.
[24] Ahn, T., and Mote, C., 1998, "Mode Identification of a Rotating Disk," Exp. Mech., **38**(4), pp. 250–254.
[25] Bucher, I., Schmiechen, P., Robb, D. A., and Ewins, D. J., 1994, "Laser-Based Measurement System for Measuring the Vibration on Rotating Discs," Proceedings SPIE 2358, 1st International Conference on Vibration Measurements by Laser Techniques: Advances and Applications, Ancona, Italy, October 3–5, pp. 398–408.
[26] Di Maio, D., and Ewins, D. J., 2011, "Continuous Scan, a Method for Performing Modal Testing Using Meaningful Measurement Parameters—Part I," Mech. Syst. Signal Process., **25**(8), pp. 3027–3042.
[27] Stanbridge, A., Martarelli, M., and Ewins, D., 2001, "Rotating Disc Vibration Analysis With a Circular-Scanning LDV," Proceedings of the 19th International Modal Analysis Conference (IMAC XIX), Orlando, FL, February 5–8, SEM, pp. 1211–1217.
[28] Bucher, I., 2004, "Estimating the Ratio Between Travelling and Standing Vibration Waves Under Non-Stationary Conditions," J. Sound Vib., **270**(1–2), pp. 341–359.
[29] Potter, R., and Gribler, M., 1989, "Computed Order Tracking Obsoletes Older Methods," SAE Technical Paper No. 891131.
[30] Shin, K., and Hammond, J. K., 2008, *Fundamentals of Signal Processing for Sound and Vibration Engineers*, Wiley, New York.
[31] Gabai, R., and Bucher, I., 2009, "Excitation and Sensing of Multiple Vibrating Traveling Waves in One-Dimensional Structures," J. Sound Vib., **319**(1–2), pp. 406–425.
[32] Minikes, A., Gabay, R., Bucher, I., and Feldman, M., 2005, "On the Sensing and Tuning of Progressive Structural Vibration Waves," IEEE Trans. Ultrason. Ferroelectr. Freq. Control, **52**(9), pp. 1565–1576.
[33] Vold, H., Herlufsen, H., Mains, M., and Corwin-Renner, D., 1997, "Multi Axle Order Tracking With the Vold-Kalman Tracking Filter," Sound Vib., **31**(5), pp. 30–35.
[34] Boashash, B., 1992, "Estimating and Interpreting the Instantaneous Frequency of a Signal. 1. Fundamentals," Proc. IEEE, **80**(4), pp. 520–538.
[35] Schmiechen, P., and Ingenieure, V. D., 1998, *Travelling-Wave Speed Coincidence*, VDI Verlag, Berlin.
[36] Bucher, I., and Ewins, D., 1997, "Multidimensional Decomposition of Time-Varying Vibration Response Signals In Rotating Machinery," Mech. Syst. Signal Process., **11**(4), pp. 577–601.
[37] Proakis J. G., 2001, *Digital Communications*, McGraw-Hill, New York.
[38] Thomas, D. L., 1979, "Dynamics of Rotationally Periodic Structures," Int. J. Numer. Methods Eng., **14**(1), pp. 81–102.
[39] Kim, M., Moon, J., and Wickert, J., 2000, "Spatial Modulation of Repeated Vibration Modes in Rotationally Periodic Structures," ASME J. Vibr. Acoust., **122**, pp. 62–68.
[40] Ewins, D., 1975, "Vibration Modes of Mistuned Bladed Disks," Proceedings of the ASME Gas Turbine Conference and Products Show, Houston, TX, March 2–6.
[41] Lamb, H., and Southwell, R., 1921, "The Vibrations of a Spinning Disk," Proc. R. Soc. London, Ser. A, **99**(699), pp. 272–280.
[42] Boashash, B., 1992, "Estimating and Interpreting the Instantaneous Frequency of a Signal. 2. Algorithms and Applications," Proc. IEEE, **80**(4), pp. 540–568.
[43] Honda, Y., Matsuhisa, H., and Sato, S., 1985, "Modal Response of a Disk to a Moving Concentrated Harmonic Force," J. Sound Vib., **102**(4), pp. 457–472.